Reflections on Shading

David Forsyth, *Member, IEEE,* and Andrew Zisserman, *Member, IEEE*

Abstract— **Mutual illumination forms a significant component of image radiance that is not modeled by the image irradiance equation. Its effects, which are easy to observe in real scenes, lead to complicated structures in radiance. Because mutual illumination is a global interaction, accounting for its effects in shape from shading schemes is impossible in the general case. We argue that as a result, dense depth maps produced by schemes that assume the image irradiance equation are intrinsically inaccurate.**

Discontinuities in radiance are well behaved (in a sense made precise in the paper) under mutual illumination and are a robust shape cue as a result. We discuss the few other such sources known at present. Throughout, these points are illustrated by images of real scenes.

Index Terms—**Computer vision, radiosity, shape from shading.**

I. Introduction

SHAPE from shading is critically dependent on a simple photometric model, known as the image irradiance equation [19], [20]. This model is only an approximation for real scenes because it assumes that radiance is a function of a purely local geometric property: the surface normal. It ignores the fact that patches of surface reflect light not only to an imaging sensor but also to other patches of surface. This "mutual illumination" makes the distribution of radiance a complicated function of the global scene geometry.

In this paper, we demonstrate that mutual illumination can produce significant effects in real scenes. A dramatic example that illustrates the difficulties that mutual illumination presents to shape recovery schemes appears in Fig. 1. These effects are qualitatively modeled very well by the radiosity equation—a result well known in the graphics community [6], [26]. Using the radiosity equation, we predict the occurrence of special events in the radiance, namely, discontinuities in the radiance and its derivatives. Again, experimental evidence establishes the validity of this approach. Mutual illumination can generate discontinuities in the derivatives of radiance unrelated to local geometry.

We argue that it is not possible to obtain veridical dense depth or normal maps from a shading analysis. However, discontinuities in radiance are tractably related to scene geometry and, moreover, can be detected. We suggest that greater reliance be placed on these discontinuities and other sparse cues rather than on the actual values of radiance.

Manuscript received September 17, 1990; revised November 29, 1990. This work was supported by the Rhodes Trust and Magdalen College, Oxford University, and by the Science and Engineering Research Council.

The authors are with the Robotics Research Group, Department of Engineering Science, Oxford University, Oxford, England.

IEEE Log Number 9100892.

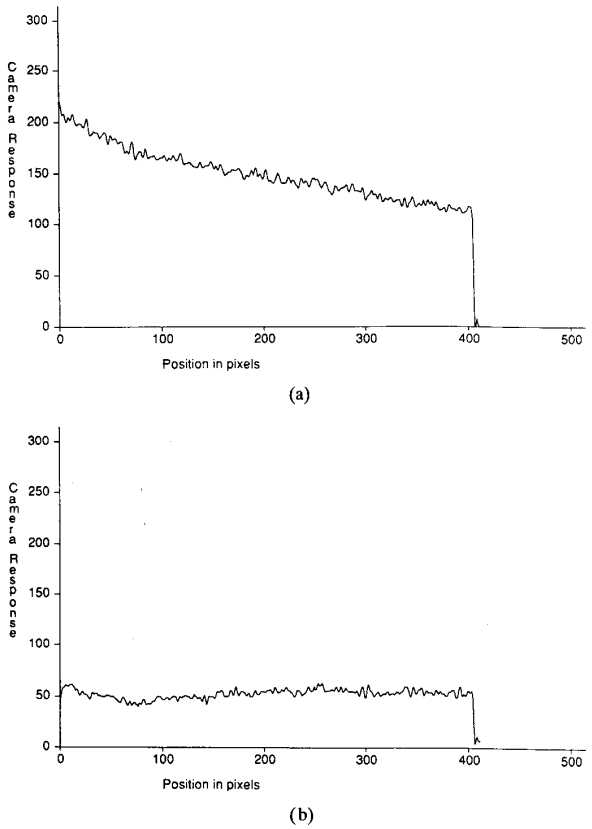

Fig. 1. (a) and (b) show the radiance measured for one white plane face of a 30° corner, illuminated down the angle bisector. In (a), the opposing face, which is not visible to the camera, was white. In (b), it was black. The camera aperture was not adjusted between images, nor was the illuminant moved. Note the dramatic differences in the radiances measured. These differences are caused by a surface that is not visible to the camera, and so it is hard to see how any algorithm for shading analysis could infer its presence and account for its effects.

II. The Radiosity Equation

Consider a scene consisting of surfaces $\boldsymbol{r}(\boldsymbol{u})$, parametrized by $\boldsymbol{u}$, where the boldface italic type denotes a vector quantity. Note that in general the surfaces will not be parametrized by image coordinates because some surfaces may be occluded or missing in the image. The radiance of the surface point parametrized by $\boldsymbol{u}$ is denoted by $N(\boldsymbol{u})$, and its albedo by $p(\boldsymbol{u})$.

The radiance at a point is the sum of two terms: the radiance resulting from the illuminant alone and the radiance resulting from light reflected off other surface patches. The second term

must be a sum over all surface patches. For Lambertian surface the radiance at u is given by

$$N(u) = N_0(u) + p(u) \int_D K(u,v)N(v)\,dv \qquad (1)$$

where D covers all the surfaces in the scene, $K(u,v)$ represents the geometrical gain factor (often called a form factor) for the component of radiance at u due to that at v, and $N_0(u)$ is the component of radiance at u due to the effects of the source alone. In what follows, we use the term "initial radiance" to refer to N_0. Equation (1), which expresses energy balance, is called the *radiosity equation* (see, for example, [6] or [25]).

When $p(u)$ is constant, (1) is a Fredholm equation of the second kind. K is referred to as the *kernel* of this equation.

For Lambertian surfaces where only diffuse reflection occurs, the kernel takes the form

$$K(u,v) = \frac{1}{\pi} \frac{(n(v)\cdot d_{uv})(n(u)\cdot d_{vu})}{(d_{uv}\cdot d_{uv})^2} View(\mathbf{u},\mathbf{v})$$

where $n(u)$ is the surface normal at the point parametrized by u, d_{uv} is the vector from the point parametrized by u to that parametrized by v; View(u,v) is 1 if there is a line of sight from u to v, 0 otherwise; and View$(u,u) = 0$.

There are several approaches for solving equations of this type (see, for example, [33]). This equation can be solved using a Neumann series, which may be interpreted in terms of systems of reflected rays—the details appear in [9].

It is worth noting that (1) is a linear operator on the initial radiance function $(N_0(u))$. Loosely, to get the radiance under a weighted sum of two light sources, compute (or measure) radiances under both separately and add the weighted results.

Numerical forward solutions of the radiosity equation for complicated geometries are relatively straightforward to construct but are computationally intense ([3], [7], [8], [13], [26], [34], and [35] is a sample of recent references). However, it is difficult to visualize the geometric effects underlying mutual illumination. We have therefore concentrated on simple scenes with a single translational symmetry. A numerical solution is obtained by integrating out the symmetry in the kernel and using finite elements in the usual way. In this case, the finite-element kernel matrix can be obtained in closed form without numerical integration (see [9]). Some closed-form solutions for the radiance for simple geometries appear in [9] and [25].

III. Mutual Illumination Examples

For small albedo, the interreflections are small, and the resulting radiance is dominated by source effects. Solutions of the radiosity equation tend in this case toward the radiance predicted by the image irradiance equation. We exploit this to demonstrate the effects of mutual illumination by comparing the radiance of a white set of objects and a black set with similar geometry. Qualitative differences in radiance distributions for images of the black and white scenes can be ascribed to the effects of mutual illumination.

A number of examples of the effects of mutual illumination appear in the figures. All images were taken with a CCD camera with its automatic gain control defeated. Objects were either of matte white paper, with no visible surface texture, or were painted with either matte white or matte black enamel spray paint. The ratio of reflectance for the white paper to paper painted black was at least 40 : 1, and the paper painted black looked deep black in bright light.

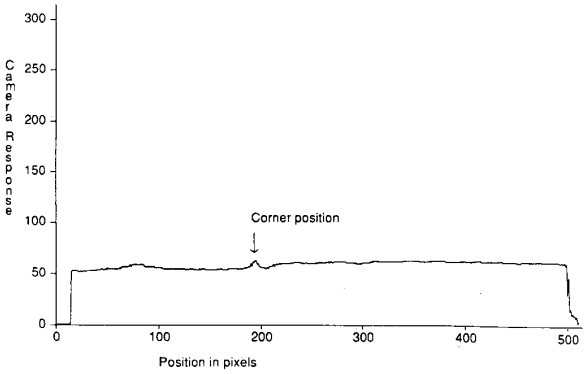

Fig. 2. A specimen control: image intensity observed across a black 90° corner, for an illuminant directed along the angle bisector. The control images ensure that effects observed were not simply a product of light source effects. The flat profile establishes that the illumination is essentially uniform across the scene. The small bump occurs because the corners were constructed by folding cardboard, with the result that there is a line of surface facets perpendicular to the camera.

It is difficult in practice to provide a point source at infinity. We therefore used a light with a large diffuser and took control images, e.g., Fig. 2, at each stage to ensure that the image intensities measured for a large, flat sheet of paper were near uniform. All graphs show image intensity plotted against distance along a section across the translational symmetry.

A. A Concave Polyhedral Corner

The scene consists of the intersection between two planar patches viewed along the angle bisector. The illuminant direction for each figure is indicated in the figure captions. It can be seen quite clearly from Figs. 2–6 that mutual illumination causes a significant qualitative effect (similar to the well-known "roof edge") in these images.

Horn [18] constructed a numerical solution to a similar equation for this geometry and obtained the typical roof-edge signature and recognized this to be a cue for concave polyhedral edges. Brady and Ponce [2] make this point as well and demonstrate the output of a roof edge finder that found a concave intersection of planar patches in this way.

In fact, the typical signature is a roof edge, or more accurately, a pair of rather broad spikes, hereafter called *reflexes*, only when the illuminant lies along the angle bisector. This is clearly shown in Fig. 3. When the illuminant lies off the angle bisector, these reflexes are superimposed on a step edge, as shown in Fig. 4. The finite-element solution to the radiosity equation is in good agreement with these cross sections. Figs. 5 and 6 show how these reflexes vary dramatically in size with albedo.

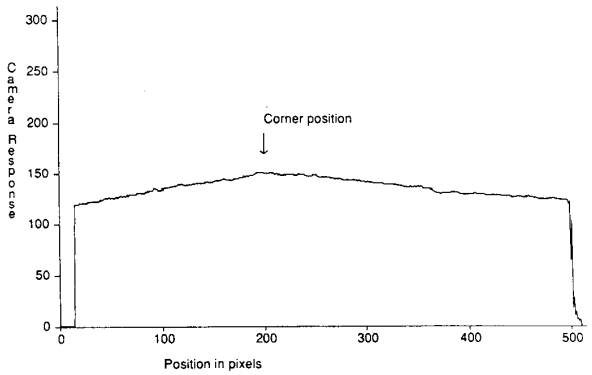

Fig. 3. Image intensity observed across a white 90° corner. The scene has the same geometry as Fig. 2 but is white instead of black. Note the pronounced roof edge.

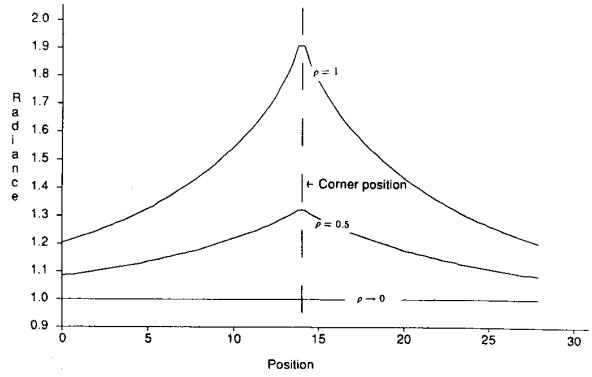

Fig. 4. Image intensity observed across a white 90° corner for an illuminant directed off the angle bisector. This is the typical shape for a concave polyhedral edge.

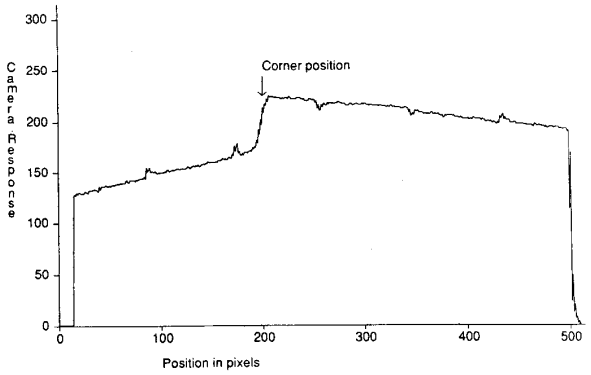

Fig. 5. Image intensity predicted using the finite- element method for a 90° corner with illuminant directed along the angle bisector over a range of albedoes. Note that the reflexes become more pronounced with albedo. The flattened top to the reflexes shown is an artifact of the display technique resulting from linking the nodal values of the constant elements employed in the finite-element program.

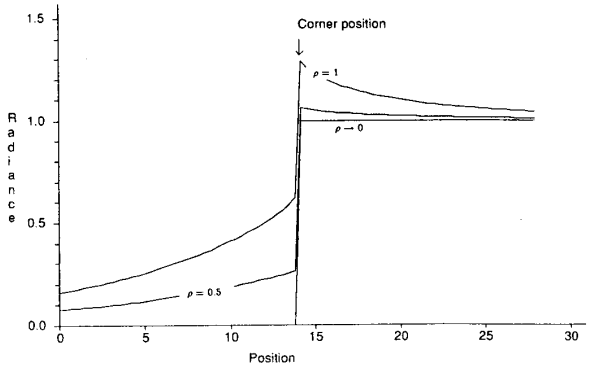

Fig. 6. Image intensity predicted by the finite-element method for a white 90° corner with illuminant directed parallel to one plane for a range of albedoes. Note that the reflexes become more pronounced with albedo.

B. Blocks World

The scene consists of polyhedral objects. Images and cross sections are shown in Figs. 7–10. Since it is hard to provide similar geometries in this case, the radiance signals must be examined with an eye to qualitative differences. In the black scene, the grey levels typically change sharply and are coupled to surface orientation in the obvious way. However, in the white scene, there are many reflexes at concave intersections. Gilchrist [11] used scenes similar to those in Figs. 7 and 8 in experiments that suggest that humans can use mutual illumination effects as a cue to surface lightness judgments.

C. A Concave Hemicylinder

Fig. 11 shows the radiance profile for a concave black cylinder on a black background—the form is broadly as expected from the image irradiance equation. Fig. 12 shows the radiance profile for a concave white cylinder on a white background. The profile is radically different from the previous case.

D. A White Convex Hemicylinder on a Plane Background

The objects consist of white convex half cylinders on a black or a white background. The geometry and terminology are illustrated in Fig. 13.

Fig. 14 shows a section of the image intensity measured for a white cylinder on a black planar background, with the camera perpendicular to the background. The light is at approximately 45° to the background. The image intensity function is as predicted by the image irradiance equation. Fig. 15 shows what happens when the black background is replaced with a white one. Notice, in particular, the large reflex where the cylinder meets the plane. This reflex demonstrates that mutual illumination can create structure in shadowed regions.

E. Summary

In general, the effects of mutual illuminations are substantial. Our experimental results agree well with those predicted by the theory, even though the numerical solution assumes that the objects have infinite extent along the symmetry axis.

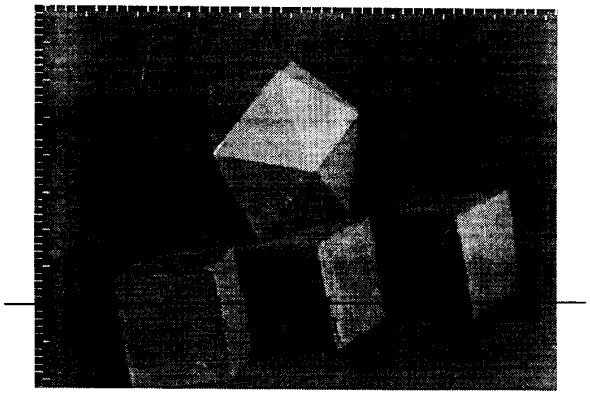

Fig. 7. Image of a scene containing black polyhedral objects. The black line indicates the section represented by Fig. 9.

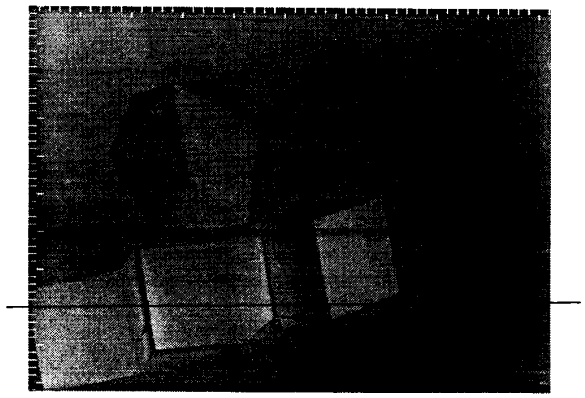

Fig. 8. Image of a scene containing white polyhedral objects. The black line indicates the section represented by Fig. 10. Notice the bright patches at the concave intersections.

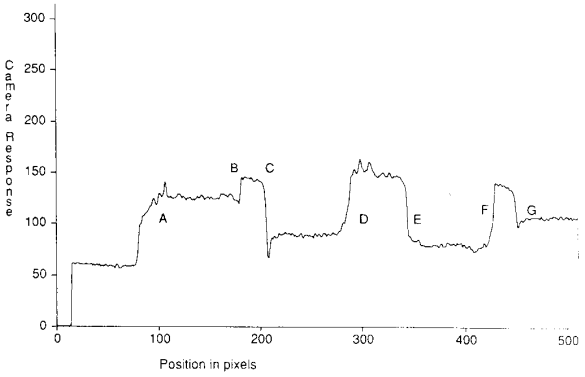

Fig. 9. Section of image intensity for Fig. 7. The radiosity events labeled line up with those marked along the line in Fig. 7. This section should be compared with that of 10 with a particular emphasis on qualitative effects. The narrow, dark spikes in this and the next section are caused by shadowing in the narrow gap between two disjoint polyhedral faces.

Mutual illumination serves to produce a rich variety of complex image features (for example, the well-known roof edges of Fig. 5 or the reflexes of Fig. 15). Radiance events resulting from surface features take a wide range of forms. Edge detectors that are optimized for one-dimensional step edges

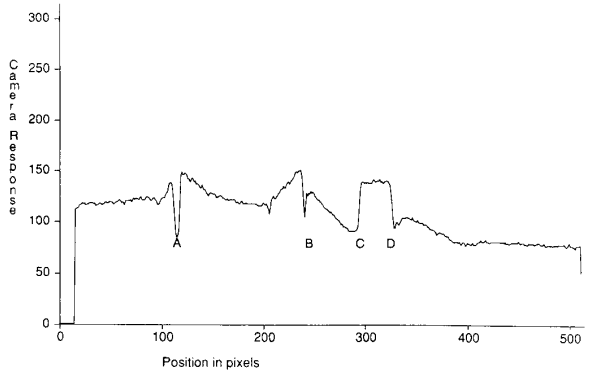

Fig. 10. Section of image intensity for Fig. 8. Notice just how pronounced the effects of the reflexes are for concave intersections. The radiosity events labeled line up with those marked along the line in Fig. 10.

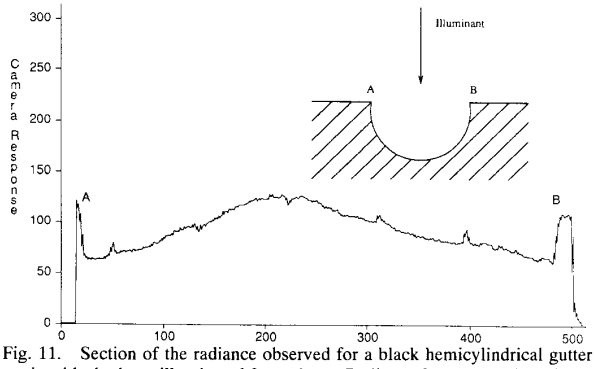

Fig. 11. Section of the radiance observed for a black hemicylindrical gutter cut in a black plane, illuminated from above. Radiance features marked A and B in this and the following figure occur at the points on the profile (shown in the inset) marked with corresponding letters.

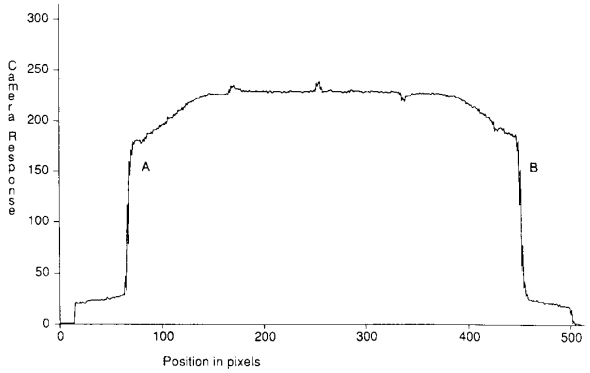

Fig. 12. A section of the radiance observed for a white hemicylindrical gutter cut in a black plane, illuminated from above. Note that this signal is qualitatively very different from that of Fig. 12. In particular, note that the constant central region is *not* a saturation effect. Quantitative shape from shading, based on the image irradiance equation, would produce entirely the wrong result with this data.

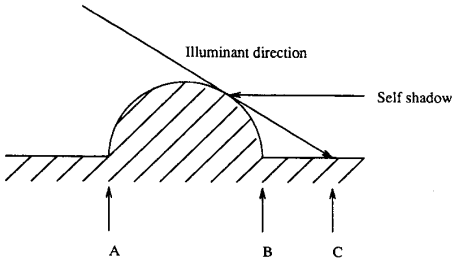

Fig. 13. Geometry for convex half cylinder on planar background, showing illuminant direction, self-shadowed region, and cast shadow. The illuminant was at an angle of about 45° to the background plane.

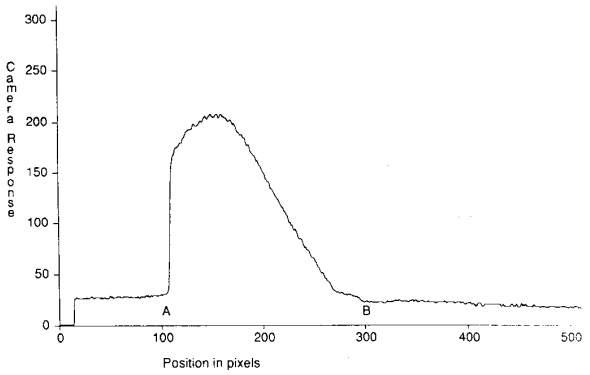

Fig. 14. Measured radiance for a convex white half-cylinder on a *black* background as in Fig. 13. The self-shadow is evident as a discontinuity in radiance derivative at pixel 280.

are not normally very successful at detecting or localizing richer image structures. Descriptions of the detailed structure of a discontinuity may themselves provide useful three-dimensional shape information. For example, the structure of the discontinuity in radiance at a convex polyhedral edge is very different from that at a concave polyhedral edge. There is a substantial scope for further work in documenting, detecting, and interpreting "canonical" features in image radiance (some contributions appear in [31]; [30] explicitly considers mutual illumination).

IV. Predicting Radiance Events

The examples in the previous section demonstrate that the radiosity equation is a better model of image radiance formation than the image irradiance equation. This section investigates the shape information that can be extracted using this model. Analyzing this equation is in general very difficult because of the complicated way in which shape appears. No useful constraints on the radiance itself are known in general. However, it is possible to predict the behavior of discontinuities in radiance and its derivative under mutual illumination. The behavior of these radiance features is closely coupled to scene geometry in a relatively simple way.

We assume that all surfaces are piecewise smooth and Lambertian. No specular reflection occurs. In this case, it

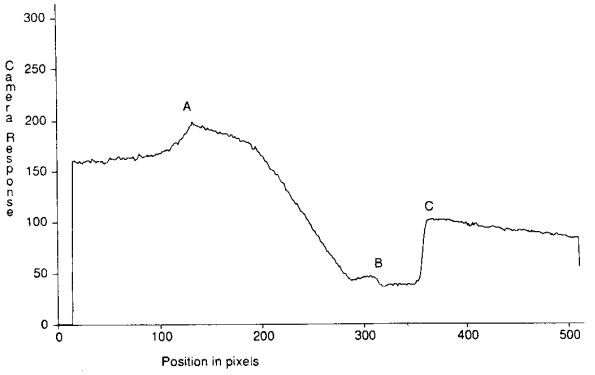

Fig. 15. Measured radiance for a convex white half cylinder on a *white* background as in Fig. 13. The radiance features labeled A, B, and C occur at the points with the corresponding labels in Fig. 13. There is a discontinuity in radiance at B, which would not be predicted by the image irradiance equation, and one at C, caused by a shadow. Note the almost cusp-like peak caused by the mutual illumination at the concave intersection A. Note self shadow at pixel 280.

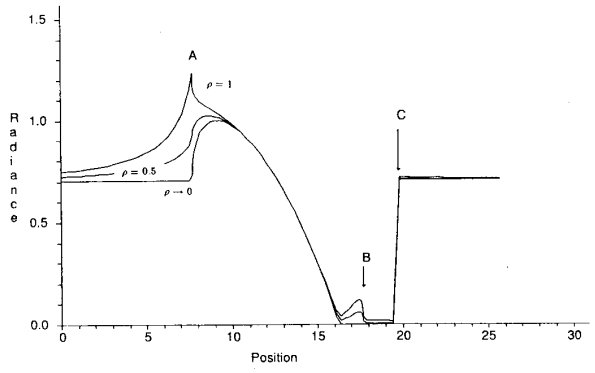

Fig. 16. Image intensity predicted using finite-element method for a convex half cylinder on a background of the same albedo for a range of albedoes. There is very good agreement with the intensity observed for this geometry (Fig. 15). Note self shadow at position 16.

is possible to prove the following results for the radiosity equation.

Discontinuities in Radiance—Discontinuities in radiance are well behaved in the sense that they appear at points where the first derivative of the surface is discontinuous, at discontinuities in surface reflectance, or at cast-shadow edges. In other words, the image irradiance equation is as good as the radiosity equation for predicting the position of discontinuities in radiance but may not predict their magnitudes correctly.

Discontinuities in Radiance Derivatives—Discontinuities in the derivative of radiance appear where the image irradiance equation predicts them and at a number of other points, where the image irradiance equation predicts a continuous derivative. The "new" discontinuities in the derivative of radiance are essentially an occlusion effect. An illuminated surface patch acts as an extended light source, and occluding such a source generates a discontinuity in the derivative of radiance on the shadowed surface.

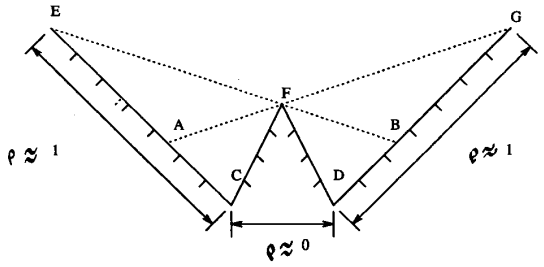

Fig. 17. In this simple geometry, there is a discontinuity in the derivative of radiance at points A and B due to mutual illumination. This can be predicted using the COG in Fig. 19.

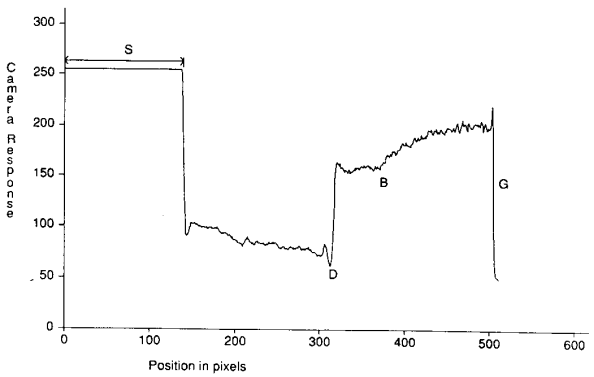

Fig. 18. A section of the radiance observed for a geometry similar to that of Fig. 17. Note the fast change in derivative of radiance marked at point B, corresponding to point B in Fig. 17. The experiment consisted of imaging a paper figure lit so that one of the faces was very bright. The other face then displayed the predicted fast change in derivative. The bright face (the region of the profile marked S) saturated the camera so that the effect corresponding to point A in Fig. 17 is not visible.

The proof of both these results appears in [10], which introduced a device called the crease occlusion graph (COG) that catalogs the discontinuities in the kernel graphically. In turn, this makes it possible to analyze the discontinuities in the radiance and its derivatives in terms of relatively simple geometric effects. Fig. 19 given below shows an example of a COG for a simple geometry. The method of proof of these results makes is possible to show that discontinuities in the derivatives of radiance arise from mutual illumination in a highly ordered fashion. In particular, they occur in a predictable way when surfaces occlude one another. This encourages speculation that these discontinuities could also represent shape cues.

A. Experimental Examples

These results show that discontinuities predicted from the radiosity equation *cling to surface features*. An example of this effect is given by the reflex in Fig. 15. Discontinuities predicted by the image irradiance equation may be local (for example, changes in albedo) or global (for example, shadows) in origin. Mutual illumination can accentuate, diminish, or even possibly, for highly unlikely geometries, null out these discontinuities.

Discontinuities in one of the derivatives of initial radiance occur, for example, at self shadows—where the illuminant direction grazes the surface. The discontinuities in the derivative of radiance predicted by the radiosity equation are often small and hard to localize, but they can be observed. Figs. 17 and 18 show a simple geometry and a discontinuity in the derivative of radiance due to mutual illumination, predicted for this geometry using the COG of Fig. 19 and observed in a real scene.

V. Implications for Shape Representation

Conventional shape from shading clearly requires that radiance be a function of surface normal alone. However, when mutual illumination is present, radiance is a global function of scene geometry. We have seen that mutual illumination causes substantial changes in the radiance. Even under controlled conditions, unless all surfaces are nearly black or the scene consists of an isolated convex surface, the effects of mutual illumination are significant.

A. Example: Mutual Illumination Effects Disturb Surface Reconstruction

Consider Fig. 18. The underlying geometry that gave this radiance is shown in Fig. 17. We consider the plane face on which the discontinuity in derivative at B falls. The radiance in Fig. 18 for this face is roughly constant from D to B, then rises roughly linearly. We have already shown that it is possible to obtain the marked discontinuity in the derivative of radiance. To predict the output of a shape from shading scheme on this image, we consider the image irradiance equation, where there is a translational symmetry. The outline is (locally, at least) a function of a single variable $z(x)$.

Given a Lambertian surface with the only light source at the viewer and the radiance normalized so that a patch perpendicular to the source direction has radiance ρ, the radiance becomes

$$N(x) = \frac{\rho}{\sqrt{1 + z'(x)^2}}. \tag{2}$$

This is a nonlinear ODE that can be solved directly given $N(x)$ as a function of x. In particular, if $N(x) = cx + d$, then

$$N(x) = \frac{1}{c}\left\{\sqrt{\rho^2 - (cx+d)^2} + \rho \log\left\{\frac{\rho - \sqrt{\rho - (cx+d)^2}}{cx+d}\right\}\right\}. \tag{3}$$

We illustrate schematically the solution for the intensity profile of Fig. 17 in Fig. 20. Even though the surface is actually planar, the reconstructed surface would contain a discontinuity in the derivative and be curved on one side of this discontinuity. All meaningful geometry in the surface has been lost by this perturbation.

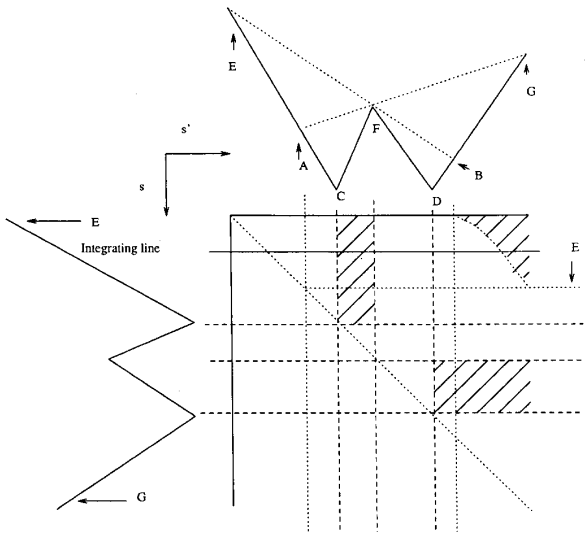

Fig. 19. The radiosity equation can be written as $N = N_0 + \boldsymbol{K}N$, where $\boldsymbol{K}$ represents the linear operator associated with the kernel. The COG charts the events that may cause discontinuities to appear in $\boldsymbol{K}N$ and its derivatives. We show this graph for a simple profile. A point (s, s') in the square represents a pair of points on the profile, which is drawn above and to the left of the graph. Regions where the corresponding points have a line of sight (i.e., $View(s, s' = 1)$) are hatched, and regions where they do not are left blank. The dashed lines are creases on the surface (discontinuities in surface orientation). Because the graph is symmetric about the line $s = s'$, only the upper half is shown. $(\boldsymbol{K}N)(s_0)$ is given by $\int K(s_0, s')N(s')\,ds'$, that is, by integrating along a line $s = s_0$. This line is referred to as the integrating line. Discontinuities in $\boldsymbol{K}N$ can then be obtained by considering the change in integrand as the integrating line sweeps down the graph. The dominant effect here is the way the support of the integrand changes—at a discontinuity, the support changes discontinuously, and $\boldsymbol{K}N$ can be discontinuous, e.g., at C. Thus, $N_0 + \boldsymbol{K}N$ can be discontinuous. To obtain discontinuities in derivative requires more analysis. By expanding the derivative of $\boldsymbol{K}N$, we see the discontinuities in the derivative of radiance can arise from the boundaries in the COG, where *View* discontinuously flips from 0 to 1. In particular, at $s = E - \epsilon$, the derivative of radiance contains a term due to a δ-function on the boundary. At $s = E + \epsilon$, this term is missing. This effect causes the discontinuity in the derivative of radiance observed in Fig. 18. Details appear in [10]

B. Accuracy of Recovered Surfaces

This example illustrates that assuming the image irradiance equation in the presence of mutual illumination will lead shape from shading to produce inaccurate surface reconstructions. Other shape techniques assume the image irradiance equation will be similarly affected. The following are examples:

- The photometric invariants described by Koenderink and Van Doorn [24] do not apply to objects where mutual illumination effects are manifest as this approach relates the singular behavior of the field of isophotes to that of the Gauss map by assuming that radiance is purely a function of the Gauss map.
- Photometric stereo techniques (Horn [19] is a good general reference for these techniques) are adversely affected by mutual illumination. It is known that gain due to mutual illumination can cause some surface patches to be brighter than is consistent with the photometric model [21], [22]. However, if photometric stereo techniques are used with more than two light sources, the reconstructed surface normal is overconstrained, and it is possible to estimate its error and delineate regions that have been adversely affected by mutual illumination. This approach will deliver a representation that is dense in patches. A judicious arrangement of light sources can reduce the effects of mutual illumination, although it is unclear whether this offers a worthwhile advantage in practice.

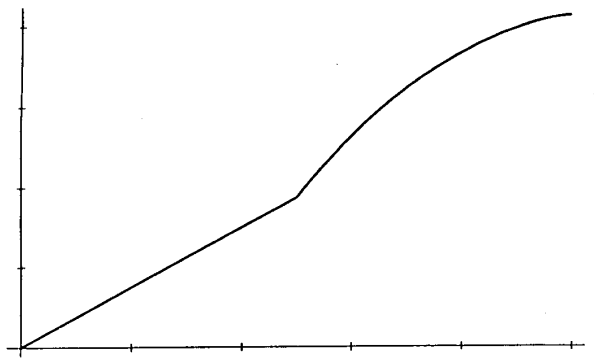

Fig. 20. Schematic of the shape reconstructed for the radiance shown in Fig. 18 using the methods for one-dimensional shape from shading described in the text.

Recently, Nayar *et al.* [28] have demonstrated a scheme that iteratively updates shape estimates to account for mutual illumination effects. They show that for simple cases, the scheme converges. They acknowledge (see p. 18 of [28]) that the scheme does not always converge on complicated examples. A major difficulty with this scheme lies in an important aspect of mutual illumination; distant surfaces, which are not visible to the imaging device, may make substantial contributions to image radiance if the form factor linking them to the surfaces viewed is sufficiently large. It is not, in general, possible to account for these contributions. Fig. 1 shows two sections of image intensities taken from two images of precisely the same geometry with precisely the same lighting—the only difference is that in the second image, a nearby surface, which is invisible to the camera, has been covered with black paper. As the figure demonstrates, mutual illumination from this invisible surface has significantly changed the image intensities.

C. The Value of Shading Information

If the goal of a shading analysis is just a dense depth map, then its success must be judged on the accuracy of that reconstruction. This can be tested by carefully measuring a real object, imaging it under known circumstances, reconstructing its shape using shape from shading, and comparing the resulting depth map with the shape of the original object. We are not aware of any such tests that deal with scenes other than isolated, convex objects[1] in the literature (see [17] for a quantitative test on a sphere). Much shape from shading work tests schemes either on data simulated using the image irradiance equation (which tests only the numerical regime) or on real data but without providing "ground truth" for

[1] Both concave objects and groups of objects need investigation.

comparison. Such experimental regimes give no guide to the accuracy of the output of these schemes on real shading data.

However, photometric stereo has been successful in applications (for example, [21]). One explanation may lie in the way it has been used to match models to small model bases. In this case, a sufficiently robust representation of model shape combined with a small model base serve to compensate for patchy information from the shading analysis. This illustrates the point that it is generally not possible to evaluate shape representation schemes outside the context of some application; for particular tasks, the disruptive effects of mutual illumination may not significantly affect the performance.

D. Alternatives to Dense Depth Maps

Modifying shape from shading schemes to recover accurate, dense depth maps despite the effects of mutual illumination appears to be impossible in the general case. An alternative approach is to extract cues from radiance that are wholly or largely unaffected by radiance from distant surfaces (see also [1]). We briefly review the cues with this property.

- *Discontinuities in Radiance and Its Derivatives:* These features bear a tractable relationship to scene geometry. However, it does not seem possible to exploit this relationship for discontinuities in the derivatives of radiance because they appear hard to detect stably.
- *Shadows:* Since a shadow region is bounded by discontinuities in radiance and the derivatives of radiance, its boundary will be unaffected by mutual illumination. This makes it possible to interpret pools of shadow on a surface using a simple geometric model by applying, for example, the techniques of [14], [15], and [23]. Unfortunately, it is difficult at present to detect pools of shadow on surfaces reliably.
- *Grooves and Pits:* Koenderink and Van Doorn [25] suggest considering properties of the radiance signal that are tractably coupled to shape and yet are largely invariant to changes in illumination. The example they cite consists of a small deep hole or a groove in a surface. At such a feature, there will be an attached shadow for almost any illuminant. Intuitively, this is because it is hard to choose a lighting direction that will illuminate the inside of the groove or hole. A simple example is given by the lines on human foreheads, which are often geometrically small but are made visually prominent under a wide range of illuminants by this shadowing effect.

VI. Conclusion

We have shown that mutual illumination produces significant effects in real scenes and that these effects can be modeled (at least qualitatively) by the radiosity equation. Our data imply that existing algorithms for shading analysis are unlikely to compute accurate surface reconstructions in complex scenes.

However, discontinuities in radiance and its derivatives behave well under mutual illumination. Discontinuities in radiance can be predicted using the image irradiance equation. Predicting discontinuities in the derivative requires both the image irradiance equation and an occlusion analysis. These localization results are abstract. In practice, edge detectors [4] respond to large derivatives rather than to discontinuities. We have shown that in real scenes, discontinuities are often surrounded by a complicated structure in the radiance signal. As a result, the *detected* position of a discontinuity may vary slightly from that predicted using the image irradiance equation.

The localization results treat only the existence of discontinuities—we have no result bounding the effects of mutual illumination on the derivatives of radiance. Our model has assumed that all surfaces are Lambertian, but the results on the position of discontinuities assume only that the bidirectional radiance distribution function is continuous. In fact, little is known about the effects of large lobes in the BRDF on radiosity solutions. Work by Tagare [32] suggesting that a wide range of surfaces are best modeled by a three-lobed BDRF opens a range of interesting problems for shading analysis.

The great complexity of the interactions involved in mutual illumination mean that an exhaustive mathematical analysis is unlikely. However, shading contains shape cues; the important issue is how to sidestep the effects of mutual illumination and determine which cues are reliable, robust, and tractably coupled to surface shape.

Acknowledgment

The authors are most grateful to A. Blake, J. Mundy, and R. Woodham for a number of helpful discussions and insightful suggestions. The paper was improved by the careful comments of an anonymous referee. They also thank M. Brady and C. Brown for help, discussions, and encouragement. P. Hubel provided measurements of relative surface lightness.

References

[1] A. Blake, A. Zisserrman, and G. Knowles, "Surface descriptions from stereo and shading," *Image Vision Comput.*, vol. 3, pp. 183–191, 1985 (also included in [20]).
[2] J. M. Brady and J. Ponce, "Toward a surface primal sketch," MIT AI-Memo 824, MIT AI Lab, Cambridge, MA, 1985.
[3] D. R. Baum, H. E. Rushmeier, and J. M. Winget, "Improving radiosity solutions through the use of analytically determined form-factors," in *Proc. SIGGRAPH '89,* 1989, pp. 325–334.
[4] J. F. Canny, "Finding edges and lines in images," *IEEE Trans. Patt. Anal. Machine Intell.*, vol. PAMI-8, pp. 679–698, 1986.
[5] B. Carrihill and R. Hummel, "Experiments with the intensity depth ratio sensor," *CVGIP,* vol. 32, pp. 337–358, 1985.
[6] M.F. Cohen and D. P. Greenberg, "The hemi-cube: A radiosity solution for complex environments," in *Proc. SIGGRAPH '85,* 1985, pp. 31–40.
[7] M.F. Cohen D. P. Greenberg, D. S. Immel, and P. J. Brock, "An efficient radiosity approach for realistic image synthesis," *IEEE Comput. Graphics Applicat.,* pp. 27–35, Mar. 1986.
[8] M. F. Cohen, S. E. Chen, J. R. Wallace, and D. P. Greenberg, "A progressive refinement approach to fast radiosity image generation," in *Proc. SIGGRAPH '88,* 1988, pp. 75-84.
[9] D. A. Forsyth and A. Zisserman, "Mutual illumination," in *Proc. CVPR,* 1989 .
[10] ——, "Shape from shading in the light of mutual illumination," *Image Vision Comput.*, vol. 8, pp. 42–49, 1990.
[11] A. L. Gilchrist, "The perception of surface blacks and whites," *Sci. Amer.*, vol. 240, pp. 112–124, 1979.
[12] A. L. Gilchrist and A. Jacobsen, "Perception of lightness and illumination in a world on one reflectance," *Perception,* vol. 13, pp. 5–19, 1984.
[13] C. M. Goral, K. E. Torrance, D. P. Greenberg, and B. Battaile, "Modeling the interaction of light between diffuse surfaces," in *Proc. SIGGRAPH '84,* 1984, pp. 213–222.

[14] M. G. Hatzitheodorou and J. Kender, "An optimal algorithm for the derivation of shape from darkness," in *Proc. CVPR,* 1988.
[15] M. G. Hatzitheodorou, "The derivation of 3D surface shape from shadows," in *Proc. DARPA Image Understanding,* 1989.
[16] G. Healy, "Local shape from specularity," in *Proc. 1st ICCV,* 1987, pp. 151–160.
[17] B. K. P. Horn, "Obtaining shape from shading information," P. H. Winston, Ed., in *The Psychology of Computer Vision.* New York: McGraw-Hill, 1975.
[18] ——, "Understanding image intensities," *Artificial Intell.,* vol. 8, pp. 201–231, 1977.
[19] ——, *Robot Vision.* Cambridge, MA: MIT Press, 1986.
[20] B. K. P. Horn, Ed., *Shape from Shading.* Cambridge, MA: MIT Press, 1989.
[21] K. Ikeuchi, H. K. Nishihara, B. K. P. Horn, P. Sobalvarro, and S. Nagata, "Determining grasp configurations using photometric stereo and the PRISM binocular stereo system," *Int. J. Robot. Res.,* vol. 5, no. 1, 1986.
[22] K. Ikeuchi, "Determining a depth map using a dual photometric stereo," *Int. J. Robot. Res.,* vol. 6, no. 1, 1987.
[23] J. Kender and E. M. Smith, "Shape from darkness; deriving surface information from dynamic shadows," *Proc. AAAI,* 1986.
[24] J. J. Koenderink and A. J. Van Doorn, "Photometric invariants related to solid shape," *Opt. Acta.,* vol. 27, pp. 981–996, 1980.
[25] ——, "Geometrical modes as a general method to treat diffuse interreflections in radiometry," *J. Opt. Soc. Amer.,* vol. 73, pp. 843–850, 1983.
[26] G. W. Meyer, H. E. Rushmeier, M. F. Cohen, D. P. Greenberg, and K. E. Torrance, "An experimental evaluation of computer graphics imagery," *ACM Trans. Graphics,* vol. 5, no. 1, pp. 30–50, 1986.
[27] M C. Morrone and R. A. Owens, "Feature detection from local energy," *Patt. Recog. Lett.,* vol. 6, pp. 303–313, 1987.
[28] S. K. Nayar, K. Ikeuchi, and T. Kanade, "Shape from interreflections," Int. Rep. CMU-RI-TR-90-14, Carnegie-Mellon Univ., Pittsburgh, PA, 1990
[29] B. O'Neill, *Elementary Differential Geometry.* New York: Academic, 1966.
[30] D. E. Pearson and J. A. Robinson, "Visual communication at very low data rates," *Proc. IEEE,* vol. 74, no. 4, pp. 795–812, 1985.
[31] P. Perona and J. Malik, "Detecting and localizing edges composed of steps, peaks and roofs," presented at 3rd Int. Conf. Comput. Vision, 1990.
[32] H. Tagare, "A theory of photometric stereo for a general class of reflectance maps," in *Proc. CVPR,* 1989, pp. 38–45.
[33] F. G. Tricomi, *Integral Equations,* New York: Dover, 1985.
[34] J. R. Wallace, M. F. Cohen, and D. P. Greenberg, "A two-pass solution to the rendering equation: A synthesis of ray tracing and radiosity methods," in *Proc. SIGGRAPH '87,* 1987, pp. 311–320.
[35] J. R. Wallace, K. A. Elmquist, and E. A. Haines, "A ray tracing algorithm for progressive radiosity," in *Proc. SIGGRAPH '89,* 1989, pp. 315–324.

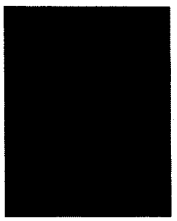

David Forsyth (S'87–M'88) received the B.Sc. degree in 1984 and the M.Sc. degree in 1986, both in electrical engineering from the University of the Witwatersrand, Johannesburg, South Africa. He received the D.Phil. degree in 1989 from Oxford University, Oxford, England.

He currently holds a prize Fellowship at Magdalen College, Oxford. His research interests include computer vision, computer algebra, and algebraic geometry.

Andrew Zisserman (M'86) received the B.A. degree in theoretical physics and part III mathematics, all from Cambridge University, Cambridge, England. In 1984, he received the Ph. D. degree.

From 1984 to 1987, he was an Alvey-funded Research Fellow at the University of Edinburgh, Edinburgh, Scotland. He is currently an SERC Advanced Research Fellow in the Robotics Research Group, Oxford University. His research interests are in robot vision, especially qualitative vision and applications of invariance. He has published a number of papers in this area as well as a book with A. Blake, *Visual Reconstruction* (MIT Press).